Structural investigation of thin films and multilayers using X-ray scattering

Satish Vitta

Department of Metallurgical Engineering and Materials Science, Indian Institute of Technology-Bombay, Mumbai 400 076, India

A non-destructive characterization of the structure in nanostructured thin films and multilayers is an area of significant importance. In this context the grazing incidence X-ray scattering (GIXS) technique has become a powerful tool. In the present paper the various parameters that define the structure in thin films and multialyers are discussed together with their origin. The GIXS theory relevant to determining these parameters is then discussed in brief. The applicability of the GIXS technique to various materials is clearly demonstrated through examples ranging from Pt-BN composite thin films to Ni-Nb/C multilayers to organic multilayers made from Cd-arachidate and Zn-arachidate (metal substituted fatty acid salts). The structural parameters of these thin films and multilayers were determined using GIXS irrespective of their nature – inorganic or organic, indicating the suitability of this method for 3-dimensional structural characterization.

IN the last two decades significant technological advances have been made towards the realization of low dimensional structures, 'nanostructures', from a range of materials. Nanostructures have physical sizes typically larger than individual atoms but significantly smaller than most of the bulk solids. The large interest in studying such low dimensional nanostructures stems from two main reasons:

(1) Scientific – The structure and physical properties of materials in general are strong functions of size or specific surface area and they change drastically with decreasing size.
(2) Technological – The changing properties with decreasing size offer the possibility of novel devices for applications ranging from information technology to biomedical engineering.

The main factor which has facilitated realization of nanoscopic structures is the advancement in methods for their preparation like physical vapour deposition and chemical vapour deposition[1–3]. Another method which has made significant advances in making organic nanostructures is the Langmuir–Blodgett (LB) technique. Using this method a variety of organic materials have been made with typically ~ 10^{-9} m as one of the physical dimensions[4,5].

e-mail: svitta@met.iitb.ernet.in

A complete understanding of the physical properties of these nanostructures requires careful structural analysis at length scales ranging from the atomic, 10^{-10} m to the microscopic, 10^{-6} m. The techniques currently used for this purpose are high resolution transmission electron microscopy, force mircoscopies (atomic and magnetic), tunnelling microscopy and ion scattering. The transmission electron microscope provides information from very small volumes over short length scales, 10^{-10} m to 10^{-8} m. This technique is extremely powerful in providing atomic/molecular level structural information but is not suited to provide information over the entire length scale of physical features. It is also destructive in nature since it needs an extremely thin electron transparent sample for investigation. The force microscopies and the tunnelling microscopy on the other hand are non-destructive and are capable of providing information over the complete length scale. However they are sensitive to the surface alone and do not provide sub-surface or buried structural information. Ion scattering technique on the other hand, provides information from both surface and subsurface structural features depending on the probing ion beam energy. It has been used to determine chemical composition and crystal quality both in bulk solids and thin films. This technique however does not provide long length scale, > 10^{-8} m, and structural information such as topography/morphology of surfaces/interfaces which are crucial in many applications. Recently however X-ray scattering is being used increasingly for the characterization of nanostructures, both solid and liquid, at all the different length scales. This is because in the last decade significant technological developments have taken place in understanding the phenomenon of X-ray scattering from surfaces coupled with technological developments in the field of generation of powerful X-ray beams[6–10]. This has made X-ray scattering as one of the unique techniques for the study of surfaces, interfaces and buried structures. The other advantages of the X-ray scattering technique as a tool to investigate the structure of nanoscopic materials are:

(1) Its capability to provide averaged quantitative information over the length scales 10^{-10} m to 10^{-6} m from relatively large volumes.
(2) Its non-destructive nature and the technique does not need any special sample preparation.
(3) It is versatile to study even liquid surfaces.

This technique, however, provides structural information via the reciprocal space and not the real space like the various microscopy techniques. The real space structure, however can be determined by understanding the X-ray scattering behaviour of surfaces/interfaces.

In the present paper the application of X-ray scattering technique for studying the surfaces and interfaces in nanometer-sized thin films and multilayers is reviewed. This is because of the dominant role played by thin films and multilayers, both inorganic and organic, in advanced technology devices. Next, a brief theoretical background to the problem of X-ray scattering from surfaces and interfaces is presented. The experimental facilities required for structural studies using X-ray scattering technique are then mentioned followed by typical case studies ranging from inorganic to organic materials. Finally, a summary of the methodology together with the current status is given.

Brief theoretical background

The surface/interface morphology in thin films and multilayers made using any of the deposition/layer transfer techniques will be far from being smooth or featureless because of the stochastic nature of the various deposition processes. These processes introduce features on an otherwise smooth substrate during the process of growth over the entire length scale ranging from the atomic, 10^{-10} m, to microscopic, 10^{-6} m (refs 11–13). Such features can vary the physical properties significantly and hence the morphology, atomic to microscopic, has to be completely characterized to understand these changes in properties. Figure 1 shows a schematic diagram of the typical structure of a surface/interface formed in a multilayer as a result of growth from the vapour phase of two materials

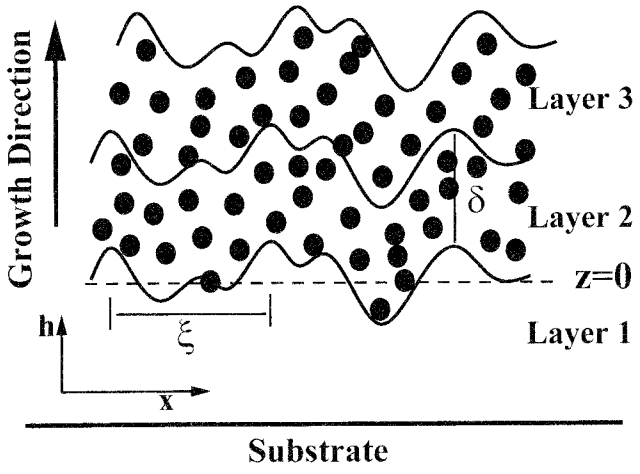

Figure 1. Schematic representation of the non-planar interface morphology in thin films and multilayers that develops as a result of growth. The height fluctuations around the mean position $z = 0$, are characterized by the roughness σ which has both lateral and vertical correlation lengths given by ξ and δ, respectively. Circles in the layers represent atoms/molecules present in the individual layers.

on each other. The various parameters that define the 3-dimensional structure in thin films are, density of the thin layers ρ, thickness of the layers t, roughness or surface height fluctuation over the average position σ, typical correlation length of roughness in the plane of the surface ξ, vertical replication length of the interface morphology in the case of multilayers δ, and atomic or molecular arrangement, periodic/non-periodic, in the individual layers.

The density of materials deposited from the vapour phase onto a cold substrate in general will be far less than the bulk value. This is because of diffusional restraints for atomic movement on the substrate surface which introduce defects such as vacancies and voids. Elimination of these defects is a function of total film thickness and temperature. Consolidation of the structure takes place as either the film thickness increases or as the substrate temperature increases during deposition leading to densification. However the overall film thickness of interest to advanced electronic devices is $< 10^{-6}$ m and in this thickness range the film density will always be lower than the bulk value unless deposition is done onto a highly elevated temperature substrate. Hence the density of the film ρ becomes a defining parameter of the structure of thin films.

The vapour phase deposition processes introduce surface height fluctuations/roughness starting with growth on a flat surface. The roughness σ increases with increasing thickness of the film before reaching a saturation value. These fluctuations are statistically correlated in the plane of the surface and this correlation length also increases with film thickness before reaching a saturation value. In order to describe such a rough surface/interface in terms of a random variable z defined as the deviation of the interface from its mean position, $[h(x, y) - \langle h(x, y)\rangle]$, where $\langle\, h(x, y)\,\rangle$ is the ensemble average of heights, several model surface profile functions are used in literature. They vary from the most commonly found error function profile to the step function profile and are applicable to surfaces produced by different processes like vapour growth, interdiffusion, etc.[14]. For the specific case of an error function profile, which is commonly observed in many growth processes, the distribution of surface heights $z(x, y)$ about the average plane, $z = 0$, is a Gaussian function given by the relation:

$$P(z) = \frac{1}{\sqrt{2\pi\sigma^2}} \exp\left(-\frac{z^2}{2\sigma^2}\right), \tag{1}$$

where $\sigma = [\langle z\rangle^2]^{1/2} = [\langle h(x, y) - \langle h(x, y)\rangle\rangle^2]^{1/2}$ is the root mean square roughness and is given by the width of this distribution. The height fluctuations develop correlations in the plane defined as the typical lateral distance ξ over which the heights of two points become statistically uncorrelated. These two quantities, σ and ξ, are related via

the height–height correlation function $C(R)$, where R is the relative distance between a pair of points on the surface. Several types of correlation functions have been proposed but the one most often used for solid surfaces is given by the relation[15]:

$$C(R) = \sigma^2 \exp\{-(R/\xi)^{2h}\}, \quad (2)$$

where $0 < h < 1$ is known as the roughness exponent and defines the nature of roughness. Surfaces with small values of h are known to have an extremely jagged profile while surfaces with h values approaching 1 are known to be made of smooth hills and valleys.

In the case of multilayers another correlation length exists and this refers to the morphological profiles of consecutive interfaces. If the morphological profiles of all the interfaces are identical or the interfaces are fully replicated, then the profile function will be unique and will be given by equations such as eq. (2). For the case of completely uncorrelated interfaces the interface profile functions will be distinct and statistically uncorrelated. The vertical replication length δ for the completely correlated case will be equal to the total thickness of the multilayer and for completely uncorrelated interfaces $\delta = 0$. In reality, however, δ takes values between these two bounding limits and is generally referred to as partially correlated interfaces.

The scattering of radiation from surfaces and interfaces is directly related to the magnitude of roughness and its spatial distribution. Hence a careful analysis of the scattering behaviour provides morphological information of surfaces and interfaces. The radiation scattered by rough surfaces/interfaces can be divided into two components – the specular component and the diffuse component. The specular component of scattered radiation is associated with equality of the angles of incidence (θ_i) and exit (θ_e) and hence is often referred to as the reflectivity. The diffuse scattering however can occur in any direction above the sample surface including the specular direction[16]. The specular component of scattering is sensitive to the average variation of electron density across the interfaces and hence an analysis of specular scattering will yield information regarding the density ρ, layer thickness t and interface roughness σ. Experimentally however only t or the repeating unit thickness in the case of multilayers can be determined. For the determination of the other morphological parameters, the specular scattering behaviour has to be numerically simulated. The specular scattering simulation is generally performed using Fresnel's optical formalism as applied to a single film. However, an extension of the single film formalism to the case of many layers using Parrat's recursive approach is more general as it can be used both for single layer films and multilayer films[17]. The amplitude reflectivity from $(j - 1/j)$th interface in the case of homogeneous layers with sharp interfaces is given as:

$$r_{j-1,j} = a_{j-1}^4 \left[\frac{(r_{j,j+1} + F_{j-1,j})}{(1 + r_{j,j+1} F_{j-1,j})} \right], \quad (3)$$

where $F_{j-1,j}$ is the Fresnel coefficient of reflection for the $(j - 1/j)$th interface and a_j the amplitude factor for half the layer thickness d_j given by the relation,

$$a_j = \exp\left[-\frac{i\pi d_j}{\lambda_j (n_j^2 - \cos^2\theta_j)^{1/2}} \right]. \quad (4)$$

Here λ_j is the radiation wavelength in the jth layer, n_j the index of refraction of the jth layer and θ_j the angle of incidence in the jth layer. In reality, however, chemically and morphologically sharp interfaces can never be obtained and they will always be associated with diffuseness due to chemical interdiffusion and/or morphology. This diffuse nature of the surfaces attenuates the reflectivity and hence has to be considered for the purposes of simulation. The Gaussian functional form for the height difference distribution, eq. (1), is generally used to treat the case of non-ideal or rough surfaces/interfaces.

The lateral correlation length of the roughness ξ, the roughness exponent h and the vertical replication factor of roughness δ cannot be determined from the specular scattering behaviour. They can be determined from the diffuse scattering behaviour using the Born approximation (BA) or the distorted wave Born approximation (DWBA). The BA to predict the diffuse scattering behaviour breaks down for small values of the angle of incidence or at the total reflection region. Hence it has been extended by DWBA to include the total reflection region. The cross-section for diffuse scattering within the framework of DWBA theory is given as[7]:

$$\left(\frac{d\sigma}{d\Omega} \right) = \frac{A \left| k_0^2 (1 - n)^2 \right|}{16\pi^2} \left| T(k_1) \right|^2 \left| T(k_2) \right|^2 S(\mathbf{q}), \quad (5)$$

where A is the illuminated area on the sample, k_0 the magnitude of the wave vector $2\pi/\lambda$, and $T(k_1)$ and $T(k_2)$ are the Fresnel transmission coefficients for total reflection of the incident and exit radiation and $S(\mathbf{q})$ is the structure factor. The structure factor for diffuse scattering from surfaces is given by the relation:

$$S_{diff}(\mathbf{q}) = \frac{\exp-(q_z^2 \sigma^2)}{q_z^2} \iint (\exp[q_z^2 C(R)] - 1) \exp-(iq_x X + iq_y Y)\, dR, \quad (6)$$

where q_x, q_y and q_z are the momentum transfer vectors along the three directions and $R = (X^2 + Y^2)^{1/2}$. The diffuse scattering structure factor $S_{\text{diff}}(\mathbf{q})$ for the case of multilayers with partially correlated or uncorrelated interfaces has

an extra term representing the vertical morphological replication and is given as[18]:

$$S_{\text{diff}}(\mathbf{q}) = \frac{1}{q_z^2} \sum_{i,j=1}^{N} \Delta\Omega_i \Delta\Omega_j$$

$$\exp\left[-\frac{q_z^2}{2}(\sigma_i^2 + \sigma_j^2)\right] \exp(iq_z[z_i - z_j])$$

$$\iint (\exp[q_z^2 C_{ij}(R)] - 1) \exp -[iq_x X + iq_y Y]\, dR, \quad (7)$$

where $\sigma_{i/j}$ is the i/jth interface roughness, $\Delta\Omega_{i/j}$ the electron density contrast across the interface and $C_{ij}(R)$ the lateral correlation function of the different interfaces. For diffuse scattering from completely correlated interfaces this equation reduces to the single surface diffuse scattering case and the structure factor reduces to eq. (6). It can be seen clearly from the above eqs (6) and (7) that the diffuse scattering cross-section or the diffuse scattered intensity distribution in space is a function of the surface/interface morphology, σ and $C_{ij}(R)$.

Although a combination of specular and diffuse scattering analysis provides morphological information down to 10^{-10} m length scales, the technique is not sensitive to atomic/molecular arrangement, periodic/non-periodic, in the thin films. In order to obtain information regarding the exact atomic/molecular arrangement within the thin films grazing incidence diffraction (described next in the article) has to be performed. The conventional Bragg diffraction rules are applicable in this regime to obtain crystallographic information from within the thin films.

Experimental facilities and methods

The typical thickness of a layer will be < 100 nm either in single layer or multilayer thin films of importance to advanced technology devices. The magnitude of the corresponding wave vector **q** will be ≤ 0.06 nm^{-1}. Such low scattering vectors can be realized only in grazing incidence geometry and hence the technique is often referred to as Grazing Incidence X-ray Scattering (GIXS). Another point to be noted is the X-ray penetration depth which depends on the radiation wavelength λ, the optical constant of the material and the angle of incidence θ_i through the relation[19],

$$l = \text{penetration depth} = \frac{K \sin\theta_i}{2\mu}, \quad (8)$$

where K is a constant in the range 3.00 to 6.9 and μ is the linear absorption coefficient of the material. It can be seen from eq. (8) that the penetration depth increases with increasing angle of incidence θ_i. Hence in order to keep the phenomenon of scattering to within the thin film, the angle of incidence should be kept as low as possible. It should however be noted here that eq. (8) is not valid for incident angles less than the critical angle for total reflection θ_c. The experimental facility to perform such grazing incidence scattering requires a highly monochromatic, collimated, bright X-ray source. The X-ray sources typically used vary from the conventional X-ray tubes to rotating anodes to synchrotron produced X-ray beams. The brightness of the X-ray beam produced by a rotating anode source is $\approx 10^4$ times greater than that produced by conventional tubes. The X-ray beams produced by synchrotrons are by far the brightest possible sources with extreme monochromaticity and collimation. The brightness of the X-ray beam produced by the European Synchrotron Radiation Facility is typically six to nine orders of magnitude higher compared to the rotating anode sources. The main advantage of using very bright sources is that the magnitude of the diffuse scattered beam will be relatively high adding to better statistics and the experimental time can be considerably reduced. In general, the X-ray beam characteristics required to perform grazing incidence scattering can be defined as: wavelength resolution $\Delta\lambda/\lambda \leq 10^{-3}$; incident beam divergence, $\leq 0.05°$; and exit beam divergence, $\leq 0.1°$. A typical GIXS arrangement is shown schematically in Figure 2.

The specular scattering behaviour can be probed by the longitudinal θ–2θ scan or the reflectivity scan. This is an equiangular scan wherein the angle of incidence θ_i is always equal to the angle of exit θ_e and the net momentum transfer is in the scattering plane along a direction perpendicular to the sample surface, q_z. The diffuse scattering behaviour on the other hand can be probed by 3 different types of scanning geometries[20], shown schematically in Figure 3. They are: offset longitudinal θ–2θ scan, transverse or rocking scan, and detector scan. In the offset longitudinal scan, the sample surface with respect to the incident beam is offset from the zero position by a known angle and then a longitudinal θ–2θ scan is performed. As

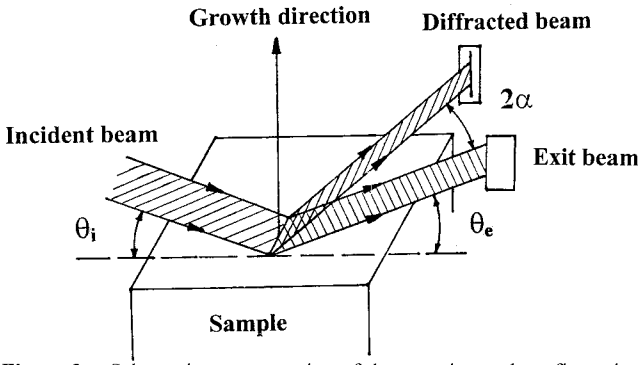

Figure 2. Schematic representation of the experimental configuration used to probe the GIXS from interfaces.

a result, the diffusely scattered intensity along a direction inclined by the offset angle to the sample surface normal is probed in the $q_z - q_x$ reciprocal space. In the transverse or rocking scan, the detector is kept at a fixed angle $2\theta = \theta_i + \theta_e$, and the angle of incidence is varied from 0° to $2\theta°$. In reciprocal space this scan realizes only the transverse or q_x component of momentum transfer at fixed values of q_z. In the case of the detector scan the angle of incidence θ_i is kept constant and the detector is scanned through a range of exit angles θ_e. This scan is similar to the offset θ–2θ longitudinal scan as it scans the $q_z - q_x$ space. The trajectory of this scan however will be curved while the offset longitudinal scan will have a straight line trajectory as shown in Figure 3. The deviation from $q_x = 0$ line for a fixed value of q_z is much more in the case of the detector scan when compared to that in the offset longitudinal scan. Hence the offset longitudinal scan is performed more often than the detector scan which requires a high brilliance X-ray source.

In order to determine the periodic/non-periodic arrangement of atoms/molecules in the layers, grazing incidence diffraction (GID) geometry has to be used[21]. In this geometry the angle of incidence is kept close to the angle of total reflection so that the incident beam penetration is restricted to the layer thickness alone. The intensity scattered in a plane, which is out of the plane of reflection, is then detected at typical scattering angles 2α in the range 10° to 80°. The momentum transfer in this type of scan is normally represented as $q_{\parallel} = \sqrt{(q_x^2 + q_y^2)}$. The scattering vector **q** has components along the three orthogonal directions x, y and z and are given by the relations:

$$q_x = \frac{2\pi}{\lambda}(\cos\theta_i \cos 2\alpha - \cos\theta_e), \tag{9}$$

$$q_y = \frac{2\pi}{\lambda}(\sin 2\alpha \cos\theta_e), \tag{10}$$

$$q_z = \frac{2\pi}{\lambda}(\sin\theta_i + \sin\theta_e). \tag{11}$$

Typical case studies

Some typical results on structural characterization of thin films and multilayers using GIXS are presented here. The results are discussed in terms of specular scattering and diffuse scattering in order to highlight the various structural parameters that can be obtained by analysing these scattering components. The specular and diffuse scattering results from various types of multilayers presented here were obtained using CuK_α radiation from a sealed tube source. The GID scans, however, were performed with a synchrotron X-ray source.

Specular scattering

The specular scattering results from both thin films and multilayers, inorganic and organic, are shown in Figure 4. The Pt-BN composite thin film of ~ 34 nm thickness was deposited by rf-sputtering technique onto a silicon crystal substrate. Pt and BN were sputtered from separate high

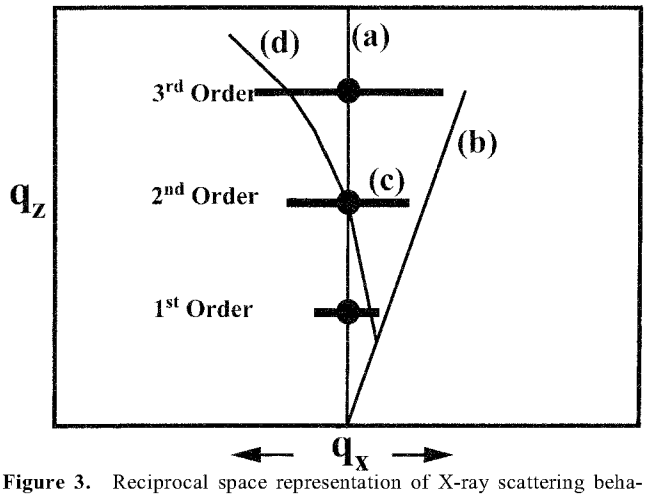

Figure 3. Reciprocal space representation of X-ray scattering behaviour from rough surface/interfaces. Horizontal lines in the reciprocal space representation correspond to scattered intensity distribution in the q_z–q_x plane at different orders of reflection from multilayers with non-ideal (rough) interfaces. (a), (b), (c) and (d) refer to longitudinal, offset longitudinal, transverse and detector scan trajectories respectively.

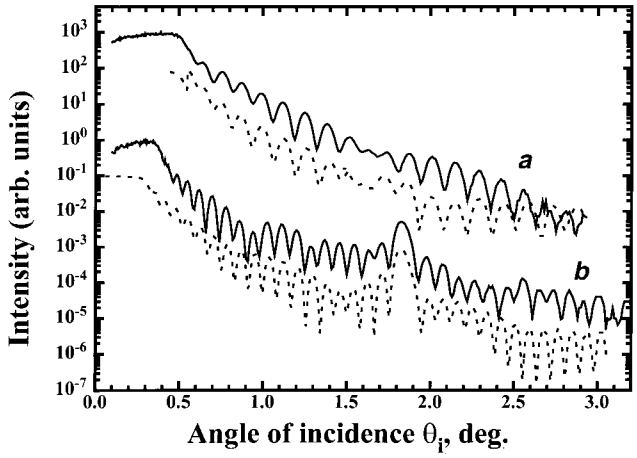

Figure 4. Longitudinal specular reflectivity from (*a*) Pt-BN composite thin film, and (*b*) $Ni_{50}Nb_{50}/C$ amorphous multilayers. Specular reflectivity from the Pt–BN composite thin film shows intensity oscillations originating from film thickness while that from $Ni_{50}Nb_{50}/C$ shows a peak corresponding to the repeat period in the multilayer along with thickness oscillations. Dotted curves below the reflectivity scans show the simulation results.

purity sources. The X-ray reflectivity from this composite thin film (Figure 4 *a*), could be measured over 6 orders of magnitude in intensity and up to an angle of incidence of 3.5°, clearly indicating the presence of a uniformly thick layer with smooth interfaces. The reflectivity shows oscillations arising due to interference of scattered X-rays from the air/thin film and thin film/substrate interfaces. The exact thickness of the thin film can be determined from the separation of these oscillations and is found to be 32.5 nm compared to 34 nm estimated from the deposition process. Apart from these oscillations, a second modulation with the node at ~ 1.6° θ_i can also be clearly seen in the figure. This second longer period oscillation indicates the presence of a Pt rich over layer on the top surface of the film with a thickness of 1.9 nm obtained from a simulation of reflectivity behaviour of the composite film, shown by the dotted line in Figure 4 *a*[22]. The presence of two separate layers in this thin film indicates compositional non-uniformities in the form of depletion of BN towards the end of the deposition process. It is known that BN is difficult to deposit by sputtering and is highly sensitive to changes in the sputtering conditions.

The reflectivity from multilayers made of amorphous $Ni_{50}Nb_{50}$ and amorphous C is shown in Figure 4 *b*. These multilayers were prepared by pulsed laser ablation deposition from pure elemental targets under ultra high vacuum conditions. The reflectivity indicates a peak at 1.87° θ_i corresponding to a bilayer period of 2.41 nm. The total film thickness oscillations can also be clearly seen and the total thickness of the multilayers is found to be 48 nm corresponding to 20 repeating periods of a-$Ni_{50}Nb_{50}$ and a-C. A simple two-layer model consisting of a-$Ni_{50}Nb_{50}$ and a-C was, however, found to be insufficient to simulate the reflectivity behaviour by using eq. (3). Assuming the presence of an inter-diffused/reacted layer made of $Ni_{1/3}Nb_{1/3}C_{1/3}$ at the two interfaces and also at the top and bottom of the multilayer stack, the reflectivity could be simulated to fit the experimental data well, shown by the dotted line in Figure 4 *b*. It was also found from the simulations that the density of each of these layers is below the equivalent bulk value, in agreement with the thin film growth models[23].

The X-ray scattering technique is general in nature and can be applied to even organic materials as shown in Figure 5 *a* and *b*. These organic multilayers were prepared using the LB technique. The acidic head group from the fatty acid, arachidic acid, was replaced with Cd and Zn metal ions, respectively and then transferred onto a solid substrate from the liquid phase[24,25]. The specular scattering from Cd-arachidate multilayers made on glass substrate is shown in Figure 5 *a*. The scan shows clearly five orders of reflection indicating the presence of a well-formed layered structure. The multilayer period can be determined from the position of the reflectivity peaks using the Bragg relation and is found to be 5.54 nm. The specular scattering behaviour was simulated assuming a simple two-layer model consisting of CH_2-unit organic tail and Cd-ion head respectively and using eq. (3). The interface roughness σ was found to be only 0.3 nm from the simulations[26], a value which is observed more commonly in liquid surfaces. The specular scattering scan from the Zn-arachidate multilayers (Figure 5 *b*), shows an interesting feature. A total of two sets of reflections up to the 5th order can be seen clearly, indicating the presence of two types of multilayered structures. The multilayer period for the two types was found to be 4.6 and 5.2 nm, respectively. The normal length of individual Zn-arachidate molecules is known to be ~ 2.75 nm and hence the typical bilayer period of Zn-arachidate multilayers should be 5.5 nm. The bilayer periods observed however are smaller than this value, indicating a tilted arrangement of the Zn-arachidate molecules in the multilayer. The angle of tilt away from the vertical direction can be determined using a simple geometrical relation and is found to be ~ 32° and 17° for the two bilayer periods observed, 4.6 nm and 5.2 nm, respectively. These results clearly show that the Zn-arachidate molecules are present in two types of tilted configurations in the multilayer[27].

Diffuse scattering

The distribution of diffusely scattered intensity in space from a rough surface will be different compared to that from multilayers due to the presence of repeating units in the multilayer. The scattered intensity from a rough surface will have a maximum around the specular condition, $q_x = q_y = 0$, and will decrease away from the specular condition for $q_x = q_y \neq 0$. In the case of multilayers with partially/completely replicated roughness the diffusely scattered intensity will be in the form of sheets with a

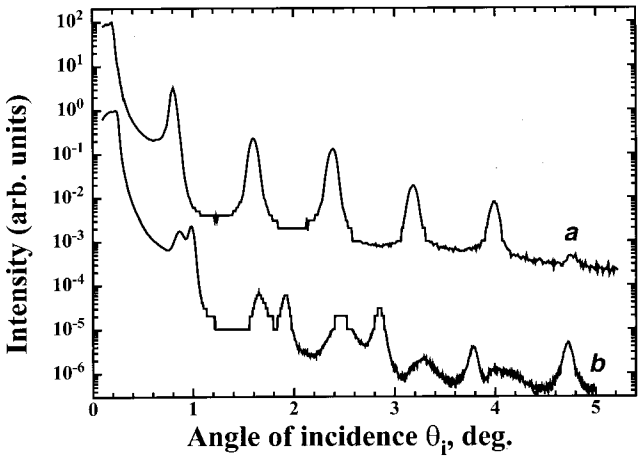

Figure 5. Specular reflectivity from (*a*) Cd-arachidate, and (*b*) Zn-arachidate. Both show peaks of increasing order, indicating the presence of a repeating layered structure. The Zn-arachidate multilayers however show two sets of reflectivity peaks, indicating the presence of two types of layered structures. Curves are vertically shifted by about two orders of magnitude for clarity.

finite width and spread around the position of reflecting maxima as shown in Figure 2. This is because the period of replicated roughness will be identical to the repeating period in the multilayer and this confines the scattered intensity to the reflectivity peak positions. The diffusely scattered intensity distribution from a multilayer with completely uncorrelated interface roughness will be similar to that from a single surface given by eq. (6). Hence the offset longitudinal scan or the detector scan is of great relevance to determine the nature of roughness correlations between different interfaces in multilayered thin films. The offset longitudinal scans from organic multilayers, Zn-arachidate and Cd-arachidate are shown in Figure 6. The scans exhibit peaks at angular positions which are coincident with the position of the peaks in the longitudinal specular scan. This indicates that the morphological features are replicated from layer to layer and that their periodicity is identical to the multilayer period d. In the case of Zn-arachidate however, (Figure 6 *a*), the two types of structures corresponding to the two separate bilayer periods exhibit different vertical replication behaviour. The shorter bilayer period, 4.6 nm, structure exhibits clear peaks up to the 5th order, indicating a large vertical replication length δ while the longer period, 5.2 nm, structure has clear peaks only up to the 3rd order, indicating a short replication length[27]. In the case of Cd-arachidate (Figure 6 *b*), clear peaks can be seen up to the 5th order, indicating a long vertical replication length δ for the interface morphology along the growth direction[26].

The diffusely scattered intensity distribution along q_x or q_y for a fixed value of q_z is a function of the surface/interface height–height or roughness correlation function $C(R)$ and hence the transverse scans are always studied in detail to determine the lateral morphological features. The transverse scans from a-$Ni_{50}Nb_{50}$/a-C and Cd-arachidate multilayers are shown in Figure 7. The transverse scan from the a-$Ni_{50}Nb_{50}$/a-C multilayer (Figure 7 *a*), was performed at the position of the first-order reflection. The scan has a strong peak in the centre corresponding to the specular position with very low scattered intensity on either sides of the specular position. The scattering behaviour simulated using the DWBA, eq. (7), indicates a short in-plane correlation length ξ of 10 nm for the 0.4 nm interface roughness σ. The interface roughness in this case, however, was found to be due to chemical interdiffusion between the components of individual layers[23]. The transverse scan from the 5th order reflection in Cd-arachidate multilayers (Figure 7 *b*), on the other hand does not exhibit a strong central specular peak and the diffuse scattering around the specular peak is also strong compared to the specular scattering itself. This type of scattering behaviour has been observed from a special class of self-affine surfaces which have small roughness with an in-plane correlation length ξ tending to ∞. The scattered intensity distribution given by eq. (5) in such cases has an analytical solution given by a Lorenztian function and the scattering from Cd-arachidate multilayers shown in Figure 7 *b* was found to follow this behaviour[26].

In all the examples discussed here the primary objective is to determine the various parameters that define the morphological features of surfaces/interfaces. The atomic/molecular arrangement in space, periodic/non-periodic, however cannot be determined using any of the above-mentioned methods. Conventionally this is done by performing what is termed as 'high angle X-ray diffraction' wherein the longitudinal θ–2θ specular scan is performed at angles of incidence $\theta_i > 20°$. The depth of penetration

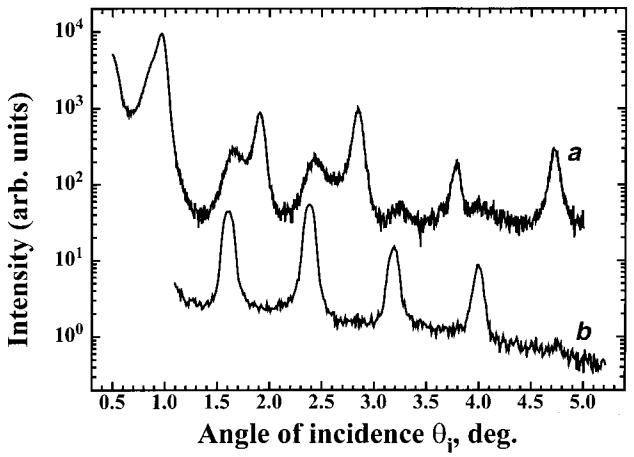

Figure 6. Offset longitudinal diffuse scattering scan from (*a*) Zn-arachidate, and (*b*) Cd-arachidate multilayers shows peaks at the position of the reflectivity peaks, indicating vertical replication of the interface morphology. The Zn-arachidate sample was offset by 0.2° from the specular condition while the offset in Cd-arachidate was 0.4°. Curves are shifted vertically by two orders of magnitude.

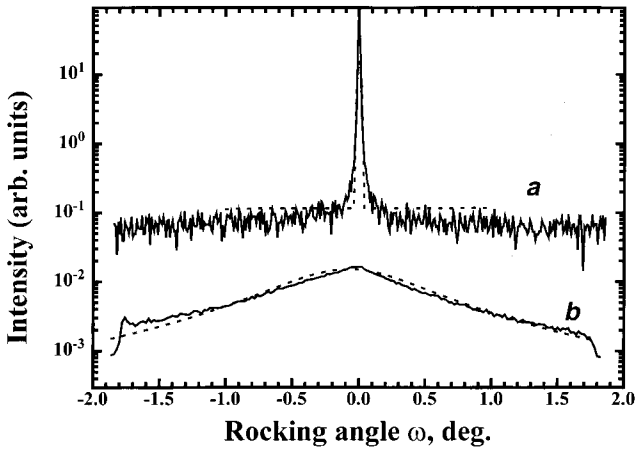

Figure 7. Transverse diffuse scattering scan from (*a*) $Ni_{50}Nb_{50}$/C multilayer, and (*b*) Cd-arachidate multilayer shows difference in morphology of the interface in the two multilayers. Transverse scan at the first-order reflection from the $Ni_{50}Nb_{50}$/C multilayer has only the specular peak in the centre with no diffuse scattering surrounding this peak, while that from the Cd-arachidate multilayers has only diffuse scattering with no strong specular peak in the centre. Transverse scan from Cd-arachidate shown here was performed at the 5th order reflectivity position. Dotted lines show results of diffuse scattering from the respective multilayers.

corresponding to such high angles of incidence will be typically > 0.5 μm, far exceeding the thickness of thin films and multilayers, wherein the thickness will be typically ≪ 0.1 μm. In such cases GID has to be performed to probe only the film structure. The GID scans from $Ni_{50}Nb_{50}$/C and Cd-arachidate multilayers are shown in Figure 8. The GID scan from the $Ni_{50}Nb_{50}$/C multilayer (Figure 8 *a*) does not show any clear peaks except for a broad peak centered at ~ 35° 2α. This clearly shows that all the layers in this multilayer have a disordered arrangement of atoms typical of an amorphous structure[23]. The molecular arrangement in Cd-arachidate multilayers however is highly periodic in space, indicated by the presence of well-defined peaks in the GID scan (Figure 8 *b*). All the peaks in this 2α spectrum could be clearly identified with an orthorhombic arrangement of the molecules.

The GIXS technique can be used to elucidate structural information not only from as-prepared thin films and multilayers but also from films which have been subjected to different processing conditions. This is shown from the two examples in Figure 9 which are from Cd-arachidate/CdS composite multilayer and the a-$Ni_{50}Nb_{50}$/a-C multilayer.

The metal substituted fatty acid multilayers in general are used as 'templates' for the preparation of 2-dimensional semiconductors. This is because the spatial location and organization of the metal atoms into sheets is well defined by the different molecular forces, and these metal atoms can be converted into semiconducting compounds by relatively simple chemical reactions. In the case of Cd-arachidate multilayers the Cd ions were converted to semiconducting CdS compound by reaction with H_2S gas. The structural changes accompanying the conversion process were characterized using GIXS. The longitudinal θ–2θ specular scattering from the H_2S exposed Cd-arachidate multilayer is shown in Figure 9 *a* and this is to be compared with the scattering behaviour shown in Figure 5 *a*. The multilayered structure is found to breakdown into two different structures with two different bilayer periods – 5.54 nm corresponding to the original Cd-arachidate multilayer period and 4.37 nm, a new structure. If the new structure is assumed to be a tilted variant of the precursor Cd-arachidate molecules, the angle of tilt can be estimated and is found to be ~ 38° away from the normal. Such tilted structures have been observed before in sulphur-based organic layers, alkanethiols, but not in Cd-arachidate/CdS composite structures. The optical spectroscopy measurements in these structures, which are sensitive to the extent of conversion of Cd to CdS, however indicate that the conversion process has reached completion. This shows that Cd is present only as CdS and not as Cd-arachidate, indicating that the layered structure with 5.54 nm as the period observed in the converted film corresponds to repeating layers of arachidic acid[28].

The a-$Ni_{50}Nb_{50}$/a-C multilayer is a prototypical mirror system to focus soft X-rays for use in a X-ray microscope. Among the several criteria that define the characteristics of such multilayer mirror systems, the structural stability both with respect to time and temperature is an important criterion. Any degradation in the layered structure will result in loss of reflectivity for the mirror system. Hence the temporal stability of the multilayer was studied using the X-ray scattering technique. The longitudinal θ–2θ specular scattering from this multilayer after a period of 2.5 years after deposition is shown in Figure 9 *b*. The multilayer during this period was kept in normal air atmosphere and no special precautions were taken to preserve the multilayer structure. The scattering behaviour is found

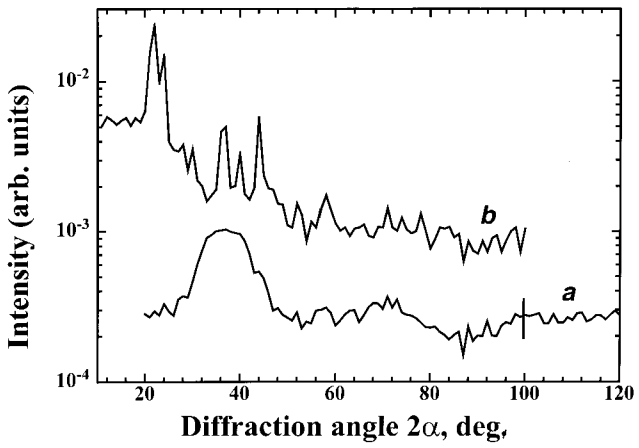

Figure 8. Grazing incidence diffraction scan from the Cd-arachidate multilayers (***b***) has several peaks while that from the $Ni_{50}Nb_{50}$/C multilayer (***a***) has only a single broad hump. This indicates the presence of strong crystallinity in the Cd-arachidate multilayers. The vertical line in (***a***) indicates the magnitude of error in the intensity values in a typical grazing incidence diffraction scan. Curves are vertically shifted.

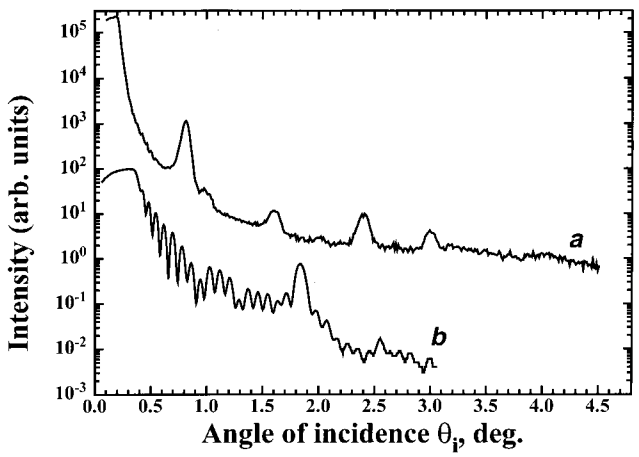

Figure 9. Longitudinal specular scattering behaviour changes completely when Cd-arachidate is exposed to H_2S gas (***a***) while it remains identical even after 2.5 years in $Ni_{50}Nb_{50}$/C multilayers (***b***). These scans indicate the structural stability when the multilayers are exposed to different conditions. Curves are vertically shifted.

to be unchanged with time when compared to that in the as-deposited condition shown in Figure 4 *b*. This indicates the high degree of temporal stability of these multilayers in spite of the presence of a large thermodynamic driving force for compositional homogenization or destruction of the layered structure[29]. The thermal stability of these multilayers at 200°C and 320°C has also been investigated using both grazing incidence X-ray reflection and diffraction. It was found that the layered structure is highly stable even after annealing at 320°C although the $Ni_{50}Nb_{50}$ layers undergo an amorphous to crystalline transformation[30].

Summary

The GIXS has emerged as a powerful technique for the characterization of 3-dimensional structure in thin films and multilayers. The technique is highly versatile in that it can be used for studying the structure of both inorganic and organic materials. The main advantage of this technique is that it can be used to extract both microscopic morphological information and atomic information in the length range 10^{-10} to 10^{-6} m in a single experiment. The limitation of this technique however is that it provides structural information in reciprocal space from which real space information has to be derived using the scattering theories. A thorough understanding of the scattering phenomenon and development of suitable theories to simulate this behaviour has made this technique a non-destructive alternative to the destructive electron microscopy technique for structural characterization.

1. Siegel, R. W., *Phys. Today*, 1993, **10**, 65.
2. Ploog, K., *Angew. Chem.*, 1988, **27**, 593.
3. Cheung, J. T. and Sankur, H., *CRC Crit. Rev. Solid State Mater. Sci.*, 1988, **15**, 63.
4. Roberts, G. G., *Adv. Phys.*, 1985, **34**, 475.
5. Zasadzinski, J. A., Viswanathan, R., Madsen, L., Garnaes, J. and Schwartz, D. K., *Science*, 1994, **263**, 1726.
6. Vineyard, G. H., *Phys. Rev. B*, 1982, **50**, 4146.
7. Sinha, S. K., Sirota, E. B., Garoff, S. and Stanley, H. B., *Phys. Rev. B*, 1988, **38**, 2297.
8. Nevot, L. and Croce, P., *Rev. Phys. Appl.*, 1980, **15**, 761.
9. Pershan, P. S., *J. Phys.: Condens. Matter*, 1994, **6**, A37.
10. Altarelli, M., Schlachter, F. and Cross, J., *Sci. Am.*, 1998, **12**, 43.
11. Bales, G. S., Bruinsma, R., Eklund, E. A., Karunasiri, R. P. U., Rudnik, J. and Zangwill, A., *Science*, 1990, **249**, 264.
12. Tong, W. M. and Williams, R. S., *Annu. Rev. Phys. Chem.*, 1995, **45**, 401.
13. Barabasi, A. L. and Stanley, H. E., *Fractal Concepts in Surface Growth*, Cambridge University Press, Cambridge, 1995.
14. Stearns, D. G., *J. Appl. Phys.*, 1992, **71**, 4286.
15. Palasantzas, G. and Krim, J., *Phys. Rev. B*, 1993, **48**, 2873.
16. Payne, A. P. and Clemens, B. M., *Phys. Rev. B*, 1993, **47**, 2289.
17. Parrat, L. G., *Phys. Rev.*, 1954, **95**, 359.
18. Sinha, S. K., *J. Phys. III France*, 1994, **4**, 1543.
19. Cullity, B. D., *Elements of X-Ray Diffraction*, Addison-Wesley, Massachusetts, 1978.
20. Savage, D. E., Kleiner, J., Schimke, N., Phang, Y.-H., Jankowski, T., Jacobs, J., Kariotis, R. and Lagally, M. G., *J. Appl. Phys.*, 1991, **69**, 1411.
21. Salditt, T., Metzger, T. H. and Peisl, J., *Phys. Rev. Lett.*, 1994, **73**, 2228.
22. Satish Vitta (to be published).
23. Satish Vitta, Metzger, T. H. and Peisl, J., *App. Opt.*, 1997, **36**, 1472.
24. Dhanabalan, A., Kudroli, H., Major, S. S. and Talwar, S. S., *Solid State Commun.*, 1996, **99**, 859.
25. Dhanabalan, A., Prashant Kumar, N., Major, S. S. and Talwar, S. S., *Thin Solid Films*, 1998, **787**, 327–329.
26. Satish Vitta, Metzger, T. H. and Major, S. S., *J. Chem. Phys.*, 1999, **111**, 11088–11094.
27. Prashant Kumar, N., Satish Vitta, Major, S. S. and Gupta, A. (to be published).
28. Satish Vitta, Metzger, T. H., Major, S. S., Dhanabalan, A. and Talwar, S. S., *Langmuir*, 1998, **14**, 1799.
29. Satish Vitta, *Mater. Sci. Eng. B*, 1999, **57**, 165.
30. Satish Vitta, *Vacuum*, 2000 (to appear).

ACKNOWLEDGEMENTS. I thank many of my collaborators, specifically T. H. Metzger, N. Prasanth Kumar, S. S. Major and A. Dhanabalan, who have contributed in these studies.

Received 18 August 1999; revised accepted 10 April 2000